



Subscriber access provided by UNIVERSITY OF CONNECTICUT

### Communication

# Giant Mechano-Optoelectronic Effect in an Atomically Thin Semiconductor

Wei Wu, Jin Wang, Peter Ercius, Nicomario Courtney Wright, Danielle Marie Leppert-Simenauer, Robert A. Burke, Madan Dubey, Avinash M. Dongare, and Michael Thompson Pettes

Nano Lett., Just Accepted Manuscript • DOI: 10.1021/acs.nanolett.7b05229 • Publication Date (Web): 20 Mar 2018

Downloaded from http://pubs.acs.org on March 22, 2018

### **Just Accepted**

"Just Accepted" manuscripts have been peer-reviewed and accepted for publication. They are posted online prior to technical editing, formatting for publication and author proofing. The American Chemical Society provides "Just Accepted" as a service to the research community to expedite the dissemination of scientific material as soon as possible after acceptance. "Just Accepted" manuscripts appear in full in PDF format accompanied by an HTML abstract. "Just Accepted" manuscripts have been fully peer reviewed, but should not be considered the official version of record. They are citable by the Digital Object Identifier (DOI®). "Just Accepted" is an optional service offered to authors. Therefore, the "Just Accepted" Web site may not include all articles that will be published in the journal. After a manuscript is technically edited and formatted, it will be removed from the "Just Accepted" Web site and published as an ASAP article. Note that technical editing may introduce minor changes to the manuscript text and/or graphics which could affect content, and all legal disclaimers and ethical guidelines that apply to the journal pertain. ACS cannot be held responsible for errors or consequences arising from the use of information contained in these "Just Accepted" manuscripts.



## Giant Mechano-Optoelectronic Effect in an Atomically Thin Semiconductor

**Authors.** Wei Wu<sup>1,2</sup>, Jin Wang<sup>2, 3</sup>, Peter Ercius<sup>4</sup>, Nicomario C. Wright<sup>1</sup>, Danielle M. Leppert-Simenauer<sup>1,5</sup>, Robert A. Burke<sup>6,7</sup>, Madan Dubey<sup>6</sup>, Avinash M. Dogare<sup>2,3</sup>, and Michael T. Pettes<sup>1,2\*</sup> **Affiliations** 

<sup>1</sup>Department of Mechanical Engineering, University of Connecticut, Storrs, CT 06269-3139, USA.

<sup>2</sup>Institute of Materials Science, University of Connecticut, Storrs, CT 06269-3136, USA.

<sup>3</sup>Department of Materials Science and Engineering, University of Connecticut, Storrs, CT 06269-3136, USA.

<sup>4</sup>Molecular Foundry, Lawrence Berkeley National Laboratory, Berkeley, CA 94720, USA.

<sup>5</sup>Department of Physics, DePaul University, Chicago, IL 60614, USA.

<sup>6</sup>U.S. Army Research Laboratory, Adelphi, MD 20783, USA.

<sup>7</sup>General Technical Services, LLC, Wall, NJ 07727, USA.

\*Corresponding author, michael.pettes@uconn.edu.

**Abstract.** Transition metal dichalcogenides (TMDs) are particularly sensitive to mechanical strain as they are capable of experiencing high atomic displacements without nucleating defects to release excess energy. Promising for photonic applications, it has been shown that as certain phases of layered TMDs MX<sub>2</sub> (M=Mo, W; X=S, Se, Te) are scaled to a thickness of one monolayer, the photoluminescence response is dramatically enhanced due to the emergence of a direct electronic band gap, compared with their multi-layer or bulk counterparts which typically exhibit indirect band gaps. Recently, mechanical strain has also been predicted to enable direct excitonic recombination in these materials, where large changes in the photoluminescence response will occur during an indirect-to-direct band gap transition brought on by elastic tensile strain. Here, we demonstrate a two orders of magnitude enhancement in the photoluminescence emission intensity

in uniaxially strained single crystalline WSe<sub>2</sub> bilayers. Through a theoretical model which includes experimentally relevant system conditions, we determine this amplification to arise from a significant increase in direct excitonic recombination. Adding confidence to the high levels of elastic strain achieved in this report, we observe strain-independent mode-dependent Grüneisen parameters over the entire range of tensile strain (1–3.59 %) which were obtained as  $1.149\pm0.027$ ,  $0.307\pm0.061$ , and  $0.357\pm0.103$  for the  $E_{2g}$ ,  $A_{1g}$ , and  $A^2_{1g}$  optical phonon modes, respectively. These results can inform the predictive strain-engineered design of other atomically thin indirect semiconductors, where a decrease in out-of-plane bonding strength will lead to an increase in the strength of strain-coupled optoelectronic effects.

**Keywords.** Strain engineering, band gap engineering, tungsten diselenide, transition metal dichalcogenide, photoluminescence, optoelectronics.

### **Main Text**

Transition metal dichalcogenides (TMDs) are a relatively new class of atomically thin materials receiving interest for overcoming limitations inherent to graphene-based electronics, of which there are more than 40 unique TMDs encompassing a diverse range of unique properties<sup>1-4</sup>. Technologies based on these materials offer size, weight, and power advantages not currently achievable using traditional materials, and are especially promising for nanophotonic applications<sup>5, 6</sup> including quantum emission sources<sup>6-16</sup>. As certain phases of layered TMDs MX<sub>2</sub> (M=Mo, W; X=S, Se, Te) are scaled to the thickness of one three-atom-thick layer, the electronic dispersion undergoes a transition from an indirect to a direct band gap due to quantum confinement effects<sup>17-20</sup>. In the TMD class, tungsten diselenide (WSe<sub>2</sub>) is particularly promising as an optoelectronic material as it can be electrostatically tuned from intrinsic to both high-electron and

high-hole concentrations and exhibits an electron-hole effective mass ratio near unity<sup>21, 22</sup>. While a direct bandgap can be intrinsically imparted in monolayer materials, it has been predicted that elastic strain<sup>23, 24</sup> can be used as an extrinsic method to reversibly engineer a direct band gap in multilayer crystals with indirect band gaps. Promising for optoelectronic applications, atomically thin WSe<sub>2</sub> has recently been shown to exhibit strain-sensitive photoluminescence (PL)<sup>25</sup> and absorbtion<sup>26</sup> responses, and localized strain has been hypothesized to enable spatially precise single photon emission<sup>8, 16</sup>. Understanding the mechanisms that are responsible for these effects, however, has been limited by difficulty in quantifying atomic-level strain experienced by an atomically thin material.

Here we report the first experimental observation of a two orders of magnitude direct excitonic recombination enhancement (124.3×) for WSe<sub>2</sub> bilayers at a 3.59% uniaxial tensile strain. This large optoelectronic response enables us to determine the strain-dependent band gap evolution by studying the indirect and direct electron transitions over a wide range of strain. Through a new *ab initio* model, we accurately reproduce the experimental strain-dependent electronic dispersion through incorporation of both van der Waals and the Poisson effect. Additionally, we have obtained mode-dependent Grüneisen parameters which allow us to validate the strain-dependent properties presented in this report.

In order to demonstrate an indirect-to-direct transition, our study focuses on single crystal bilayer WSe<sub>2</sub> which is an indirect semiconductor in its natural state. The bilayer WSe<sub>2</sub> used here is grown by a chemical vapor deposition (CVD) method similar to previous reports<sup>27, 28</sup> (see supporting information for details). In contrast to previous multilayer CVD growth reports for TMDs<sup>29</sup>, our bilayer WSe<sub>2</sub> are synthesized so that the top and bottom layers possess the same

dimensions (up to ~15  $\mu$ m). Atomic force microscopy (AFM) analysis demonstrates a uniform thickness of ~1.3 nm over the entire triangular crystallite (Figure S1, supporting information). Cross-sectional scanning transmission electron microscopy (STEM) confirms the bilayer structure with an interlayer distance of ~0.7 nm (Figure S2, supporting information). Both AFM and STEM characterizations are in accordance with the out-of-plane unit cell parameter and (0002) interlayer spacing of AB-stacked bulk WSe<sub>2</sub> (1.29825 and 0.64943 nm respectively, Powder Diffraction File no. 38-1388)<sup>30</sup>. Figure 1 illustrates that the spatially dependent Raman spectra of bilayer WSe<sub>2</sub> is uniform in intensity throughout the entire crystallite for the E<sub>2g</sub>, A<sub>1g</sub> and A<sup>2</sup><sub>1g</sub> Raman active modes.

Previous studies on strain-coupled properties of atomically thin materials have only been able to access tensile strain up to ~2 %<sup>25, 31, 32</sup> which limits optoelectronic property amplification or attenuation. One similarity is that these studies consist of an atomically thin material where only one surface is in contact with the substrate or two surfaces are in contact with two different substrate materials. This can lead to a low amount of strain being transferred from the substrate to the sample as a result of non-ideal interfacial adhesion processing or plastic deformation<sup>33</sup>. This observation erodes confidence in the reported quantitative values unless the amount of transferred strain is validated through vibrational response analysis as has been shown conclusively for graphene<sup>34</sup>. This is more critical for multilayer structures since poor interface adhesion causes a non-uniform strain distribution between the top and bottom layers which can result in slippage between layers<sup>35</sup>. Here, we have developed a method to encapsulate the atomically thin sample with poly(methyl methacrylate) (PMMA) allowing us to apply high strain values without slippage and also prevent surface degradation in our materials, which can occur by exposure to air<sup>36</sup>. CVDgrown WSe<sub>2</sub> bilayers were transferred between two ~500 nm-thick PMMA layers and attached to a ~1 mm-thick flexible poly(ethylene terephthalate) (PET) substrate (see supporting information

for details). High strain in the samples was achieved after annealing the composite at 150°C under an argon atmosphere to enhance the adhesion strength between the interfaces of PET, PMMA, and WSe<sub>2</sub> without sample degradation by exposure to air at high temperature. We observed the PMMA layer became conformal to the substrate and passed standard Scotch<sup>TM</sup> and Kapton<sup>®</sup> tape peeling tests after annealing, indicating strong adhesion, as has been observed for PMMA-assisted transfer of graphene<sup>37</sup>. We note that a recent study<sup>38</sup> found an order of magnitude increase in the thermal expansion coefficient of several monolayer TMD materials compared to the bulk material. The relationship of thermal expansion coefficient ( $\alpha$ ) to elastic modulus (E) can be expressed as  $\alpha$  =  $\gamma \rho c_v/E$ , where  $\gamma$  is the Grüneisen parameter,  $\rho$  is the mass density, and  $c_v$  is the specific heat. Since this thermophysical property is inversely proportional to the elastic constant, it is likely that monoand few-layer TMD materials are more compliant than their bulk counterparts and thus more able to be strained by bending experiments. Based on the reported values in Ref. 38, the elastic modulus of bilayer WSe<sub>2</sub> will be  $\sim$ 4.1 times smaller than the bulk value<sup>39</sup>, or  $\sim$ 12.6 GPa along the c-axis. Thus it is likely that mono- and few-layer TMD materials are more compliant than their bulk counterparts and thus more able to be strained using flexible substrates such as in this work.

Uniaxial strain in this study is applied through a custom-designed four-point bending apparatus (Figures S4–S6, supporting information), and both PL and Raman spectra are obtained using a multiline Raman spectrometer (LabRAM HR Evolution, Horiba Scientific, Ltd.). To verify the strain transferred to an atomically thin material in our experimental configuration, we first obtained the Grüneisen parameter of graphene by measuring strain-dependent Raman spectra. The graphene was transferred using the same method described for WSe<sub>2</sub>. The Grüneisen parameter,  $\gamma$ , of the inplane transverse optical (iTO) phonon polarization was determined using the 2D mode of the sample and the three-dimensional Poisson effect model described in the supporting information as

 $\gamma_{2D}$  = 3.66±0.23 (Figure S8, supporting information). This is comparable to the value we obtain for graphene by analyzing Ref. 34,  $\gamma_{2D}$ =3.583±0.267, where we have defined the uncertainty from the upper and lower 95% confidence bounds. We note that Ref. 34 has demonstrated near ideal strain transfer to graphene by comparing the experimental  $\gamma$  of the G mode ( $\gamma_{E2g}$ =1.99) with that calculated by *ab initio* modeling ( $\gamma_{E2g,DFT}$ =1.87) which add further justification to our validation approach. The slight difference between the 2D mode Grüneisen parameter in this work and in Ref. 34 arises from uncertainty in the estimated Poisson ratios for the flexible substrates used<sup>40</sup>.

The PL emission and Raman spectra of bilayer WSe<sub>2</sub> bilayer are obtained using a 2.33 eV ( $\lambda$  = 532 nm) continuous wave excitation at low power (86  $\mu$ W) to avoid sample damage and spectral shifts due to local heating effects<sup>31</sup>. Figure 2 shows the PL emission response to uniaxial tensile strain. The PL spectra were deconvolved by two Gaussian peaks which differ in energy by ~138 meV for the unstrained bilayer WSe<sub>2</sub> and by ~8 meV for a strain of 3.59 % (Figure S9, supporting information).

To elucidate the mechanisms driving the measured strain-coupled optoelectronic effects, we have developed a full theoretical analysis of the electronic dispersion evolution with strain using density functional theory (DFT), the main results of which are shown in Figure 3. Spin orbital coupling (SOC), van der Waals interaction (vdW) of WSe<sub>2</sub> layers, and the Poisson effect of the substrate are all taken into account for the electronic band structure calculation. As Fig. 3b depicts, the experimental strain-dependent indirect and direct emission peaks match well with the theoretical prediction, with only a slight difference arising from the assumption of strain-independent binding energy and the estimation of the substrate's Poisson ratio. We also compared our experimental results with a previous DFT prediction using the Heyd-Scuseria-Ernzerhof (HSE) hybrid functional which does not consider vdW interactions or the Poisson effect<sup>25</sup> (Figure 3b).

The HSE-DFT result predicted an indirect-to-direct transition crossover at a small strain of ~0.5%, which differs from our experimental and theoretical results by an order of magnitude. This large deviation indicates the importance of the vdW interaction for layered TMDs such as bilayer WSe<sub>2</sub> and the Poisson effect of the substrate in achieving physically reproducible theoretical predictions for strain-coupled transport phenomena. We note that it is reasonable to neglect the vdW interaction for un-encapsulated monolayer TMDs, however, this component is critical for multilayer TMDs.

To assign the two PL sub peaks to electronic transitions, we first compared the PL peak energy difference to the spin-orbit valence band splitting energy at the K-point in the Brillouin zone, which is  $\sim 0.5$  eV from 0 to 2% uniaxial tensile strain<sup>26</sup>. The valance band splitting energy is at least four times larger than our measured PL peak energy difference, and its dependence on strain is much less than we measured here. Secondly, neither of the two PL peaks are expected to result from trion emission since the charged exciton energy is only ~30 meV lower than the exciton energy for unstrained bilayer WSe<sub>2</sub><sup>41</sup>, which is ~4.6 times lower than we have measured. Thirdly, these two PL peaks do not belong to biexcitonic recombination since its observability should significantly diminish above 70 K<sup>42</sup>. We can also conclude that these two peaks do not stem from slippage between the top and bottom WSe<sub>2</sub> layers at high strain. As slippage will increase with strain, the difference between these two peaks would revert to a larger energy closer to that of the unstrained material, which is contradictory with our experimental observation of continuously decreasing separation with strain. As shown in the inset of Figure 2a, the unstrained PL peak at 1.50 eV has a full width at half maximum (FWHM) of 121.03 meV, which is similar to the reported FWHM of the indirect band transition of unstrained bilayer WSe<sub>2</sub><sup>43</sup>. Additionally, the straindependent blue (red) shift of the lower (higher) energy PL sub peak also matches the indirect (direct) electronic band gap strain dependence calculated by our *ab initio* model which includes spin-orbit coupling, interlayer van der Waals bonding, and the Poisson effect from the PMMA encapsulation layer (Figure 3). Thus, we assign the lower energy PL sub peak to the indirect electron transition between the conduction band minimum at the  $\Sigma$ -point (CBM $_{\Sigma}$ ) and the valence band maximum at the K-point (VBM $_{K}$ ), and the higher energy sub peak to the direct electronic transition at the K-point (CBM $_{K}$ –VBM $_{K}$ ). The PL indirect band gap linearly increased with strain at a rate of 11.14 meV/% to 1.54 eV (FWHM=123.08 meV) at 3.59% uniaxial tensile strain. The PL direct band gap decreased with strain at a rate of 27.9 meV/% from 1.64 eV (FWHM=117.2 meV) in the unstrained material to 1.54 eV (FWHM=53.6 meV) at 3.59 % uniaxial tensile strain. The FWHM of the direct transition peak is similar to that reported for mechanically exfoliated monolayer WSe<sub>2</sub> (FWHM=56 meV)<sup>43</sup>. Our theoretical model predicts that the PL indirect-to-direct crossover will occur at 4.28 %, however, the ability to reach this value experimentally is limited by the fatigue of the PMMA/PET substrate.

Since the bilayer WSe<sub>2</sub> is an indirect semiconductor at mechanical equilibrium, we report optical strain-coupled behavior for direct and indirect transitions separately. Figure 2b shows the PL intensity corresponding to the direct excitonic transition (colored squares) is enhanced by 124.3 times at 3.59% strain. The enhancement of the overall maximum PL intensity (colored triangles) is 101.4 times at 3.59% strain. Even at 1.93% uniaxial strain, the maximum PL intensity enhancement is ~42.6 times, which is 42% larger than previously reported at 2% strain<sup>25</sup> due to the high amount of strain transferred to the TMD sample in this work as verified experimentally using thin graphite (see supporting information for details). The maximum PL intensity enhancement is smaller than the enhancement of the direct transition since the indirect transition has a higher PL intensity than the direct transition for the unstrained sample. As the strain increases

to values higher than ~0.5%, the direct transition begins to dominate the PL response as shown in Figure 2a.

To elucidate the mechanisms responsible for the large enhancement observed here and to understand the maximum achievable amplification, we have used our DFT-vdW-Poisson theoretical model to calculate the enhancements of the direct and indirect excitonic transitions as

$$\frac{I_{j}(\varepsilon_{//})}{I_{j}(\varepsilon_{//}=0)} = \frac{e^{\frac{\Delta E_{j}(\varepsilon_{//})}{k_{B}T}}}{e^{\frac{\Delta E_{j}(\varepsilon_{//}=0)}{k_{B}T}}}, \quad j = \text{direct, indirect},$$
(1)

where  $\Delta E_j(\varepsilon_l)$  and  $\Delta E_j(\varepsilon_l)=0$  are the band transition energies of the strained and unstrained bilayer WSe<sub>2</sub> (see supporting information for details). The PL intensity enhancement for the experimental direct transition (colored squares in Figure 2b) and theoretical prediction results (light blue solid line in Figure 2b) are consistent. The experimental PL enhancement is 124.3 times and the calculated result is 81.35 times at 3.59% strain. The deviation at lower strain may arise from simplifying assumptions for Equation 1 and the assumption of a strain-independent binding energy in the DFT-vdW-Poisson model.

As can be seen in Figure 2b for the indirect transition, a large disagreement in both trend and magnitude between the experimental (colored triangles) and calculated (light blue solid line) amplification of the indirect transition likely arises due to enhanced scattering between K and  $\Sigma$  valleys in the conduction band, which become closer in energy with strain as will be discussed. This mechanism is also likely responsible for reducing the overall experimentally observed PL amplification in comparison with calculated amplification of the direct transition for strains above 2%. The experimental PL intensity of the indirect transition is amplified by ~59.7 times at 3.59% strain, which is contrary to both our experimental observation and theoretical prediction of an increase in indirect band gap energy with tensile strain. Applying Equation 1 to the indirect

transition, the PL intensity is expected to attenuate with tensile strain to a value of  $I_{\text{indirect}}/I_{\text{indirect}}(\varepsilon/=0) = 0.52$  at 3.59% strain. This can be explained by an increase in the phonon-assisted electron scattering from the conduction band minimum at the K-point (CBM<sub>direct</sub>) to the conduction band minimum at the  $\Sigma$ -point (CBM<sub>indirect</sub>) as illustrated in Figure 3a. The PL intensity of the indirect transition is the result of competition between: (i) an increase in the indirect band gap with strain which weakens the radiative recombination rate and (ii) phonon-assisted CBM<sub>direct</sub>-to-CBM<sub>indirect</sub> electron scattering which enhances the indirect recombination rate. The phonon-assisted CBM<sub>direct</sub>-to-CBM<sub>indirect</sub> intervalley transition rate is proportional to the direct transition rate which increases with strain. Thus, the indirect transition PL intensity is enhanced with strain. Meanwhile, increasing the indirect band gap with strain counteracts the PL intensity enhancement due to the phonon-assisted CBM<sub>direct</sub>-to-CBM<sub>indirect</sub> intervalley transitions. The energy difference between CBM<sub>direct</sub> and CBM<sub>indirect</sub> drives this intraband electron transition and can be evaluated as

$$\Delta E_{\text{CBM}_{\text{direct}}-\text{CBM}_{\text{indirect}}} = \Delta E_{\text{direct}-\text{indirect}} = E_{\text{direct}} - E_{\text{indirect}}. \tag{2}$$

Our theoretical results shown in Figure 3b indicate that  $\Delta E_{\text{indirect-direct}}$  decreases with increased strain at a rate of 35.7 meV/%, from 155 meV at  $\varepsilon_{\text{i}}$ =0% to 12.2 meV at  $\varepsilon_{\text{i}}$ =4%. Thus, the phonon-assisted CBM<sub>direct</sub>-to-CBM<sub>indirect</sub> transition rate is expected to increase with tensile strain by 250.6 times at 4% uniaxial tensile strain according to

$$\frac{I_{\text{intraband}}(\varepsilon_{//})}{I_{\text{intraband}}(\varepsilon_{//}=0)} = \frac{e^{\frac{\Delta E_{\text{CBM}_{direct}}-CMB_{\text{indirect}}}{k_{\text{B}}T}}} e^{\frac{\Delta E_{\text{CBM}_{direct}}-CMB_{\text{indirect}}}{k_{\text{B}}T}}.$$
(3)

The consequences of increased intraband scattering can be observed in Figure 2b, where the maximum PL enhancement becomes closer to the direct transition enhancement at high strain while entering into an apparent saturation regime as the valley minima near degeneracy.

Additionally, the high amplification of the indirect transition intensity with strain (as opposed to the theoretically predicted attenuation) results from the greatly increased intraband scattering processes as  $\Delta E_{\text{indirect-direct}}$  decreases towards degeneracy.

Strain-dependence of the phonon energies in bilayer WSe<sub>2</sub> yield information on atomic displacement and fundamental thermodynamic properties. Figure 4 shows the evolution of optical phonon energies with strain as obtained by Raman spectroscopy. The unstrained sample shows three major Raman active modes: (i) the in-plane transverse optical E<sub>2g</sub> mode at 250.1 cm<sup>-1</sup>, (ii) the out-of-plane transverse A<sub>1g</sub> mode at 259.5 cm<sup>-1</sup>, and (iii) the out-of-plane transverse A<sub>1g</sub> mode at 310.7 cm<sup>-1</sup>. The E<sub>2g</sub> and A<sub>1g</sub> peak energies are comparable to those reported for unstrained CVD $grown^{27}$  and mechanically exfoliated  $WSe_2$  thin layers  $^{43}$ , while the  $A_{1g}^2$  mode only appears for multilayer WSe<sub>2</sub><sup>27, 44</sup>. As increasing the uniaxial tensile strain breaks the crystal symmetry, the doubly degenerate  $E_{2g}$  mode evolves into two discrete modes,  $E_{2g}^+$  and  $E_{2g}^-$ , corresponding to the inplane atomic vibrations perpendicular and parallel to the applied strain direction, respectively. Both the  $E_{2g}^+$  and  $E_{2g}^-$  modes exhibit a consistent shift with strain (Figure 4b), indicating a lack of Raman-observable slippage between the WSe<sub>2</sub>/PMMA, PMMA/PET, and WSe<sub>2</sub>/WSe<sub>2</sub> interfaces over a large range of strain (0%-3.59%). The redshift of the  $E_{2g}$  mode arises from phonon softening in the presence of tensile strain ( $\varepsilon_{l}$ ), while the blueshift of the  $E_{2g}^{+}$  mode indicates stiffening due to perpendicular compressive strain  $(\varepsilon_{\perp\perp})$  resulting from the Poisson effect of the substrate. In contrast with previous un-encapsulated cases that only consider the in-plane two-dimensional Poisson effect<sup>34</sup>, we have evaluated the Grüneisen parameter of our encapsulated bilayer WSe<sub>2</sub> with a three-dimensional Poisson effect model developed to incorporate the compressive strain in the out-of-plane direction arising from the strained encapsulation layer. Using this threedimensional Poisson effect model, the phonon polarization specific Grüneisen parameters are evaluated as

$$\gamma_{i} = \begin{cases}
-\frac{\Delta \omega_{0,i}^{+} + \Delta \omega_{0,i}^{-}}{2\varepsilon_{//}(1 - v_{\text{in-plane}} - v_{\text{out-of-plane}})\omega_{0,i}}, & i = E_{2g} \\
-\frac{\Delta \omega_{0,i}}{\varepsilon_{//}(1 - v_{\text{in-plane}} - v_{\text{out-of-plane}})\omega_{0,i}}, & i = A_{1g}, A_{1g}^{2}
\end{cases}$$
(4)

where  $\omega_{0,i}$  is the frequency of the unstrained phonon mode i,  $\Delta\omega_{0,i}$  is the change in frequency of the phonon mode i with uniaxial strain,  $\nu_{\text{In-plane}}$  is the Poisson's ratio of the PMMA/PET composite, and  $\nu_{\text{out-of-plane}}$  is the Poisson's ratio of the PMMA (see supporting information for details). Over the range of 0–3.59% strain, the Grüneisen parameter ( $\gamma$ ) of the E<sub>2g</sub> mode is measured as 1.149 with a standard deviation of 0.027,  $\gamma$  of the A<sub>1g</sub> mode is 0.307 with a standard deviation of 0.061, and  $\gamma$  of the A<sup>2</sup><sub>1g</sub> mode is 0.357 with a standard deviation of 0.103, which are comparable with MoS<sub>2</sub><sup>31</sup>. We justify the importance of our 3D model for encapsulated atomically thin materials as follows. If we applied a two-dimensional Poisson effect model to our experimental data, the Grüneisen parameter of our samples would be calculated as 0.517±0.012, 0.138±0.027 and 0.161±0.046 for the E<sub>2g</sub>, A<sub>1g</sub> and A<sup>2</sup><sub>1g</sub> modes respectively. Thus, by neglecting the out-of-plane Poisson effect in encapsulated samples, the Grüneisen parameter would be underestimated by a factor of 2.2, which is of importance as it governs the anisotropic intrinsic phonon scattering processes in these materials<sup>45-48</sup>.

In conclusion, we have demonstrated that a two orders of magnitude photoluminescence enhancement in bilayer WSe<sub>2</sub> stems from strain-dependent electronic band gap evolution in the elastic regime. The encapsulation technique and four-point bending method developed for this

study enable us to apply up to ~3.59% uniaxial strain on our atomically thin material while preventing sample degradation from exposure to air during thermal processing and laser irradiation. We have postulated an important materials design guideline related to band degeneracy as suppression of intervalley electron scattering events through band engineering may lead to further increases in emission enhancement. Our study also demonstrates the necessity of considering van der Waals interactions and the Poisson effect in the atomically thin material's surrounding environment for theoretical predictions of strain-coupled optoelectronic phenomena.

**Supporting information available.** Additional synthesis, structural characterization, strain-validation experiment and model, and experimental details. This material is available free of charge via the Internet at http://pubs.acs.org.

Acknowledgment. The project was conceived and led by M.T.P. and W.W.; W.W. and M.T.P. conducted WSe<sub>2</sub> synthesis, experimental characterizations, and analytical modeling; J.W. and A.M.D. conducted *ab initio* theoretical modeling; W.W. and P.E. performed electron microscopy; N.C.W. and D.M.L.-S. assisted W.W. and M.T.P. in design of the four-point bending apparatus and materials synthesis; R.A.B. and M.D. synthesized the monolayer graphene used in the strain verification experiment. This work is supported by the U. S. National Science Foundation Award Numbers CAREER-1553987 (M.T.P., W.W.), REU-1461165 (D.M.L.-S.), and REU-1560098 (M.T.P., N.C.W.); a FEI Company Graduate Fellowship (W.W.); the Office of Science, Office of Basic Energy Sciences, of the U.S. Department of Energy under Contract No. DE-AC02-05CH11231 (P.E., W.W., M.T.P.); the U. S. Army Research Laboratory under Cooperative Agreement Number W911NF-14-2-0059 (J.W., A.M.D.); and the U. S. Department of Education Award P217A120249 (N.C.W.).

#### References

- 1. Geim, A. K.; Grigorieva, I. V. *Nature* **2013**, 499, 419-425. http://dx.doi.org/10.1038/nature12385
- 2. Chhowalla, M.; Shin, H. S.; Eda, G.; Li, L.-J.; Loh, K. P.; Zhang, H. *Nat. Chem.* **2013,** 5, 263-275. http://dx.doi.org/10.1038/nchem.1589
- 3. Butler, S. Z.; Hollen, S. M.; Cao, L.; Cui, Y.; Gupta, J. A.; Gutiérrez, H. R.; Heinz, T. F.; Hong, S. S.; Huang, J.; Ismach, A. F.; Johnston-Halperin, E.; Kuno, M.; Plashnitsa, V. V.; Robinson, R. D.; Ruoff, R. S.; Salahuddin, S.; Shan, J.; Shi, L.; Spencer, M. G.; Terrones, M.; Windl, W.; Goldberger, J. E. *ACS Nano* **2013**, 7, 2898-2926. http://dx.doi.org/10.1021/nn400280c
- 4. Bhimanapati, G. R.; Lin, Z.; Meunier, V.; Jung, Y.; Cha, J.; Das, S.; Xiao, D.; Son, Y.; Strano, M. S.; Cooper, V. R.; Liang, L.; Louie, S. G.; Ringe, E.; Zhou, W.; Kim, S. S.; Naik, R. R.; Sumpter, B. G.; Terrones, H.; Xia, F.; Wang, Y.; Zhu, J.; Akinwande, D.; Alem, N.; Schuller, J. A.; Schaak, R. E.; Terrones, M.; Robinson, J. A. *ACS Nano* 2015, 9, 11509–11539. http://dx.doi.org/10.1021/acsnano.5b05556
- 5. Lee, C.-H.; Lee, G.-H.; van der Zande, A. M.; Chen, W.; Li, Y.; Han, M.; Cui, X.; Arefe, G.; Nuckolls, C.; Heinz, T. F.; Guo, J.; Hone, J.; Kim, P. *Nat. Nanotechnol.* **2014,** 9, 676–681. http://dx.doi.org/10.1038/nnano.2014.150
- 6. Palacios-Berraquero, C.; Barbone, M.; Kara, D. M.; Chen, X.; Goykhman, I.; Yoon, D.; Ott, A. K.; Beitner, J.; Watanabe, K.; Taniguchi, T.; Ferrari, A. C.; Atatüre, M. *Nat. Commun.* **2016,** 7, 12978-1–6. http://dx.doi.org/10.1038/ncomms12978
- 7. Branny, A.; Kumar, S.; Proux, R.; Gerardot, B. D. *Nat. Commun.* **2017,** 8, 15053-1–7. http://dx.doi.org/10.1038/ncomms15053
- 8. Palacios-Berraquero, C.; Kara, D. M.; Montblanch, A. R. P.; Barbone, M.; Latawiec, P.; Yoon, D.; Ott, A. K.; Loncar, M.; Ferrari, A. C.; Atatüre, M. *Nat. Commun.* **2017,** 8, 15093-1–6. http://dx.doi.org/10.1038/ncomms15093

- 9. Tonndorf, P.; Schmidt, R.; Schneider, R.; Kern, J.; Buscema, M.; Steele, G. A.; Castellanos-Gomez, A.; van der Zant, H. S. J.; Michaelis de Vasconcellos, S.; Bratschitsch, R. *Optica* **2015**, 2, 347–352. http://dx.doi.org/10.1364/OPTICA.2.000347
- 10. Srivastava, A.; Sidler, M.; Allain, A. V.; Lembke, D. S.; Kis, A.; Imamoğlu, A. *Nat. Nanotechnol.* **2015,** 10, 491–496. http://dx.doi.org/10.1038/nnano.2015.60
- 11. Koperski, M.; Nogajewski, K.; Arora, A.; Cherkez, V.; Mallet, P.; Veuillen, J. Y.; Marcus, J.; Kossacki, P.; Potemski, M. *Nat. Nanotechnol.* **2015**, 10, 503–506. http://dx.doi.org/10.1038/nnano.2015.67
- 12. Chakraborty, C.; Kinnischtzke, L.; Goodfellow, K. M.; Beams, R.; Vamivakas, A. N. *Nat. Nanotechnol.* **2015,** 10, 507–511. http://dx.doi.org/10.1038/nnano.2015.79
- 13. He, Y.-M.; Clark, G.; Schaibley, J., R.; He, Y.; Chen, M.-C.; Wei, Y.-J.; Ding, X.; Zhang, Q.; Yao, W.; Xu, X.; Lu, C.-Y.; Pan, J.-W. *Nat. Nanotechnol.* **2015**, 10, 497–502. http://dx.doi.org/10.1038/nnano.2015.75
- 14. Tran, T. T.; Bray, K.; Ford, M. J.; Toth, M.; Aharonovich, I. *Nat. Nanotechnol.* **2016,** 11, 37–41. http://dx.doi.org/10.1038/nnano.2015.242
- 15. Tonndorf, P.; Schwarz, S.; Kern, J.; Niehues, I.; del Pozo-Zamudio, O.; Dmitriev, A. I.; Bakhtinov, A. P.; Borisenko, D. N.; Kolesnikov, N. N.; Tartakovskii, A. I.; de Vasconcellos, S. M.; Bratschitsch, R. *2D Mater.* **2017**, 4, 021010-1–6. http://dx.doi.org/10.1088/2053-1583/aa525b
- 16. Kumar, S.; Kaczmarczyk, A.; Gerardot, B. D. *Nano Lett.* **2015**, 15, 7567–7573. http://dx.doi.org/10.1021/acs.nanolett.5b03312
- 17. Mak, K. F.; Lee, C.; Hone, J.; Shan, J.; Heinz, T. F. *Phys. Rev. Lett.* **2010**, 105, 136805-1–4. http://dx.doi.org/10.1103/PhysRevLett.105.136805
- 18. Gutierrez, H. R.; Perea-Lopez, N.; Elias, A. L.; Berkdemir, A.; Wang, B.; Lv, R.; Lopez-Urias, F.; Crespi, V. H.; Terrones, H.; Terrones, M. *Nano Lett.* **2013,** 13, 3447–3454. http://dx.doi.org/10.1021/nl3026357
- 19. Zhao, W.; Ghorannevis, Z.; Chu, L.; Toh, M.; Kloc, C.; Tan, P.-H.; Eda, G. *ACS Nano* **2013,** 7, 791-797. http://dx.doi.org/10.1021/nn305275h

- 20. Tongay, S.; Sahin, H.; Ko, C.; Luce, A.; Fan, W.; Liu, K.; Zhou, J.; Huang, Y.-S.; Ho, C.-H.; Yan, J.; Ogletree, D. F.; Aloni, S.; Ji, J.; Li, S.; Li, J.; Peeters, F. M.; Wu, J. *Nat. Commun.* **2014,** 5, 3252-1-6. http://dx.doi.org/10.1038/ncomms4252
- 21. Fang, H.; Tosun, M.; Seol, G.; Chang, T. C.; Takei, K.; Guo, J.; Javey, A. *Nano Lett.* **2013**, 13, 1991-1995. http://dx.doi.org/10.1021/nl400044m
- 22. Yu, L.; Zubair, A.; Santos, E. J. G.; Zhang, X.; Lin, Y.; Zhang, Y.; Palacios, T. *Nano Lett.* **2015,** 15, 4928-4934. http://dx.doi.org/10.1021/acs.nanolett.5b00668
- 23. Johari, P.; Shenoy, V. B. *ACS Nano* **2012**, 6, 5449–5456. http://dx.doi.org/10.1021/nn301320r
- 24. Dong, L.; Dongare, A. M.; Namburu, R. R.; Regan, T. P.; Dubey, M. *Appl. Phys. Lett.* **2014,** 104, 053107-1-5. http://dx.doi.org/10.1063/1.4863827
- 25. Desai, S. B.; Seol, G.; Kang, J. S.; Fang, H.; Battaglia, C.; Kapadia, R.; Ager, J. W.; Guo, J.; Javey, A. *Nano Lett.* **2014**, 14, 4592–4597. http://dx.doi.org/10.1021/nl501638a
- 26. Schmidt, R.; Niehues, I.; Schneider, R.; Drüppel, M.; Deilmann, T.; Rohlfing, M.; de Vasconcellos, S. M.; Castellanos-Gomez, A.; Bratschitsch, R. *2D Mater.* **2016,** 3, 021011-1–7. http://dx.doi.org/10.1088/2053-1583/3/2/021011
- 27. Liu, B.; Fathi, M.; Chen, L.; Abbas, A.; Ma, Y.; Zhou, C. *ACS Nano* **2015**, 9, 6119–6127. http://dx.doi.org/10.1021/acsnano.5b01301
- 28. Chen, J.; Liu, B.; Liu, Y.; Tang, W.; Nai, C. T.; Li, L.; Zheng, J.; Gao, L.; Zheng, Y.; Shin, H. S.; Jeong, H. Y.; Loh, K. P. *Adv. Mater.* **2015,** 27, 6722–6727. http://dx.doi.org/10.1002/adma.201503446
- 29. Bilgin, I.; Liu, F.; Vargas, A.; Winchester, A.; Man, M. K.; Upmanyu, M.; Dani, K. M.; Gupta, G.; Talapatra, S.; Mohite, A. D.; Kar, S. *ACS Nano* **2015**, 9, 8822–8832. http://dx.doi.org/10.1021/acsnano.5b02019
- 30. Wong-Ng, W.; McMurdie, H. F.; Paretzkin, B.; Zhang, Y.; Davis, K. L.; Hubbard, C. R.; Dragoo, A. L.; Stewart, J. M. *Powder Diffr.* **1987**, 2, 257–265. http://dx.doi.org/10.1017/S0885715600012926

- 31. Conley, H. J.; Wang, B.; Ziegler, J. I.; Haglund, R. F., Jr.; Pantelides, S. T.; Bolotin, K. I. *Nano Lett.* **2013**, 13, 3626–3630. http://dx.doi.org/10.1021/nl4014748
- 32. Li, Y.; Hu, Z.; Lin, S.; Lai, S. K.; Ji, W.; Lau, S. P. *Adv. Funct. Mater.* **2016**, 27, 1616–3028. http://dx.doi.org/10.1002/adfm.201600986
- 33. Huang, M.; Yan, H.; Chen, C.; Song, D.; Heinz, T. F.; Hone, J. *Proc. Natl. Acad. Sci. U. S. A.* **2009,** 106, 7304–7308. http://dx.doi.org/10.1073/pnas.0811754106
- 34. Mohiuddin, T. M. G.; Lombardo, A.; Nair, R. R.; Bonetti, A.; Savini, G.; Jalil, R.; Bonini, N.; Basko, D. M.; Galiotis, C.; Marzari, N.; Novoselov, K. S.; Geim, A. K.; Ferrari, A. C. *Phys. Rev. B* **2009**, 79, 205433-1–8. http://dx.doi.org/10.1103/PhysRevB.79.205433
- 35. McCreary, A.; Ghosh, R.; Amani, M.; Wang, J.; Duerloo, K.-A. N.; Sharma, A.; Jarvis, K.; Reed, E. J.; Dongare, A. M.; Banerjee, S. K. *ACS Nano* **2016**, 10, 3186–3197. http://dx.doi.org/10.1021/acsnano.5b04550
- 36. Kang, K.; Godin, K.; Kim, Y. D.; Fu, S.; Cha, W.; Hone, J.; Yang, E.-H. *Adv. Mater.* **2017,** 29, 1603898-1–8. http://dx.doi.org/10.1002/adma.201603898
- 37. Suk, J. W.; Kitt, A.; Magnuson, C. W.; Hao, Y.; Ahmed, S.; An, J.; Swan, A. K.; Goldberg, B. B.; Ruoff, R. S. *ACS Nano* **2011**, *5*, 6916–6924. http://dx.doi.org/10.1021/nn201207c
- 38. Hu, X.; Yasaei, P.; Jokisaari, J.; Öğüt, S.; Salehi-Khojin, A.; Klie, R. F. *Phys. Rev. Lett.* **2018,** 120, 055902-1–6. http://dx.doi.org/10.1103/PhysRevLett.120.055902
- 39. Feldman, J. L. *J. Phys. Chem. Solids* **1976**, 37, 1141-1144. http://dx.doi.org/10.1016/0022-3697(76)90143-8
- 40. Mounet, N.; Marzari, N. *Phys. Rev. B* **2005**, 71, 205214-1–14. http://dx.doi.org/10.1103/PhysRevB.71.205214
- 41. Jones, A. M.; Yu, H.; Ross, J. S.; Klement, P.; Ghimire, N. J.; Yan, J.; Mandrus, D. G.; Yao, W.; Xu, X. *Nat. Phys.* **2014,** 10, 130–134. http://dx.doi.org/10.1038/nphys2848
- 42. You, Y.; Zhang, X.-X.; Berkelbach, T. C.; Hybertsen, M. S.; Reichman, D. R.; Heinz, T. F. *Nat. Phys.* **2015**, 11, 477–481. http://dx.doi.org/10.1038/nphys3324
- 43. Pospischil, A.; Furchi, M. M.; Mueller, T. *Nat. Nanotechnol.* **2014,** 9, 257–261. http://dx.doi.org/10.1038/nnano.2014.14

- 44. Terrones, H.; Del Corro, E.; Feng, S.; Poumirol, J. M.; Rhodes, D.; Smirnov, D.; Pradhan, N. R.; Lin, Z.; Nguyen, M. A.; Elias, A. L.; Mallouk, T. E.; Balicas, L.; Pimenta, M. A.; Terrones, M. Sci. Rep. 2014, 4, 4215-1–9. http://dx.doi.org/10.1038/srep04215
- 45. Jo, I.; Pettes, M. T.; Ou, E.; Wu, W.; Shi, L. *Appl. Phys. Lett.* **2014,** 104, 201902-1–4. http://dx.doi.org/10.1063/1.4876965
- 46. Mavrokefalos, A.; Lin, Q.; Beekman, M.; Seol, J. H.; Lee, Y. J.; Kong, H.; Pettes, M. T.; Johnson, D. C.; Shi, L. *Appl. Phys. Lett.* **2010,** 96, 181908-1–3. http://dx.doi.org/10.1063/1.3428577
- 47. Mavrokefalos, A.; Nguyen, N. T.; Pettes, M. T.; Johnson, D. C.; Shi, L. *Appl. Phys. Lett.* **2007**, 91, 171912-1–3. http://dx.doi.org/10.1063/1.2800888
- 48. Chiritescu, C.; Cahill, D. G.; Nguyen, N.; Johnson, D.; Bodapati, A.; Keblinski, P.; Zschack, P. *Science* **2007**, 315, 351–353. http://dx.doi.org/10.1126/science.1136494

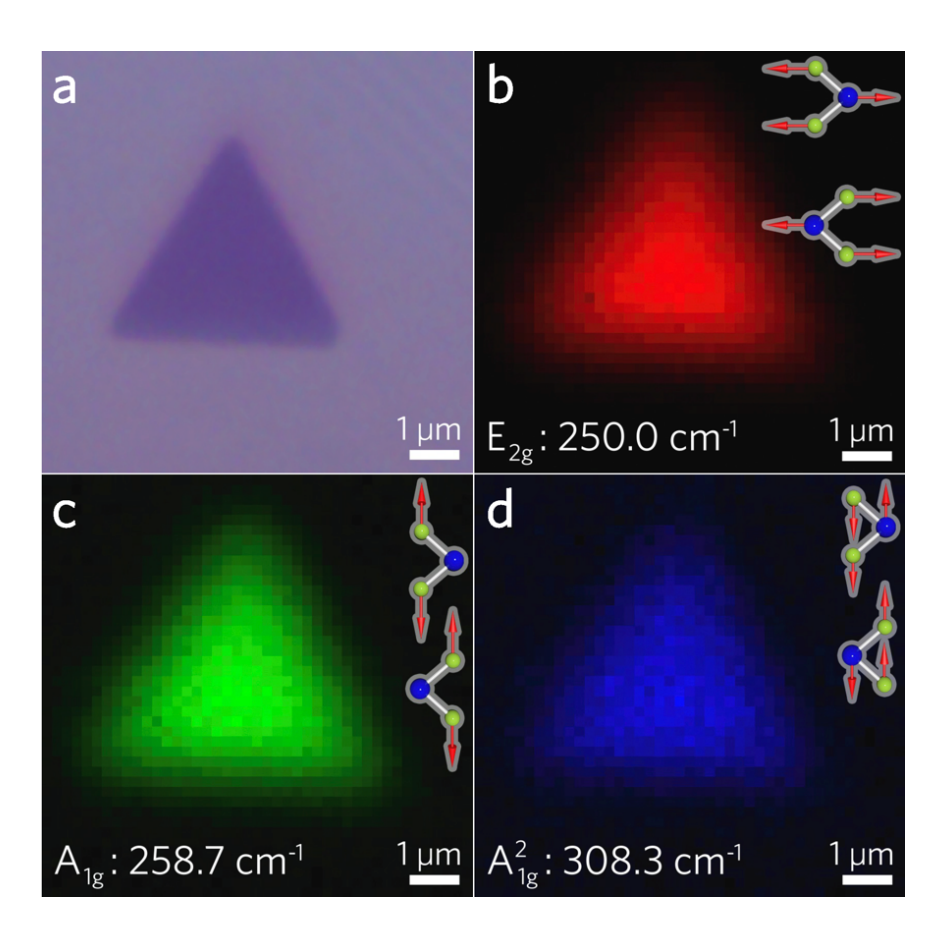


Figure 1. Spatially dependent Raman intensity of bilayer WSe<sub>2</sub>. (a) Optical image of bilayer WSe<sub>2</sub> on a 285 nm SiO<sub>2</sub>-on-Si substrate. Spatially resolved Raman intensity at (b) 250 cm<sup>-1</sup> ( $E_{2g}$  mode), (c) 258.7 cm<sup>-1</sup> ( $A_{1g}$  mode), and (d) 308.3 cm<sup>-1</sup> ( $A_{1g}^2$  mode). Vibrational modes are depicted schematically in panels (b–d).

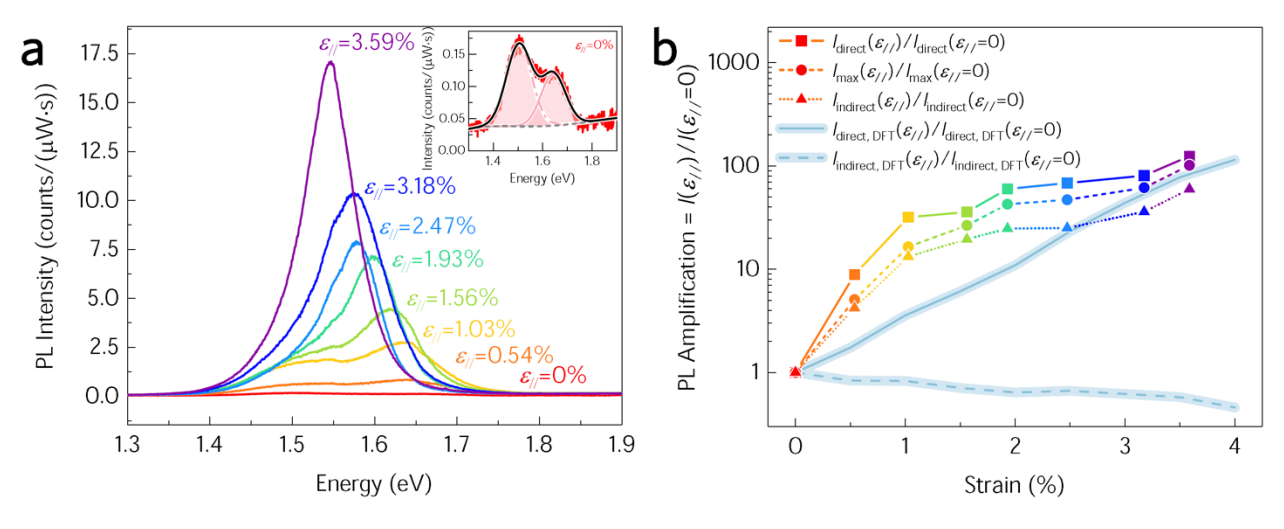


Figure 2. Amplification of the photoluminescence (PL) emission intensity of bilayer WSe<sub>2</sub> when strained up to 3.59%. (a) PL emission spectra resulting from excitation at 2.33 eV as a function of applied uniaxial strain. Inset shows the PL spectra of the unstrained material,  $\varepsilon_{\ell}=0$ , where the indirect (dash-dotted line) and direct (solid line) electronic transitions have been deconvolved using Gaussian distributions. (b) Experimental PL amplification versus strain, defined as  $I(\varepsilon_{\ell})/I(\varepsilon_{\ell}=0)$ . Subscripts max, direct, and indirect denote amplification obtained using the max intensity of the experimental PL, the max intensity of the deconvolved direct sub-peak, and the max intensity of the deconvolved indirect sub-peak, respectively. Computational results obtained by density functional theory (DFT) including the effect of spin orbit coupling, van der Waals interactions, and Poisson effect from PMMA/PET are shown for the direct (solid light blue line) and indirect (dashed light blue line) electronic transitions.

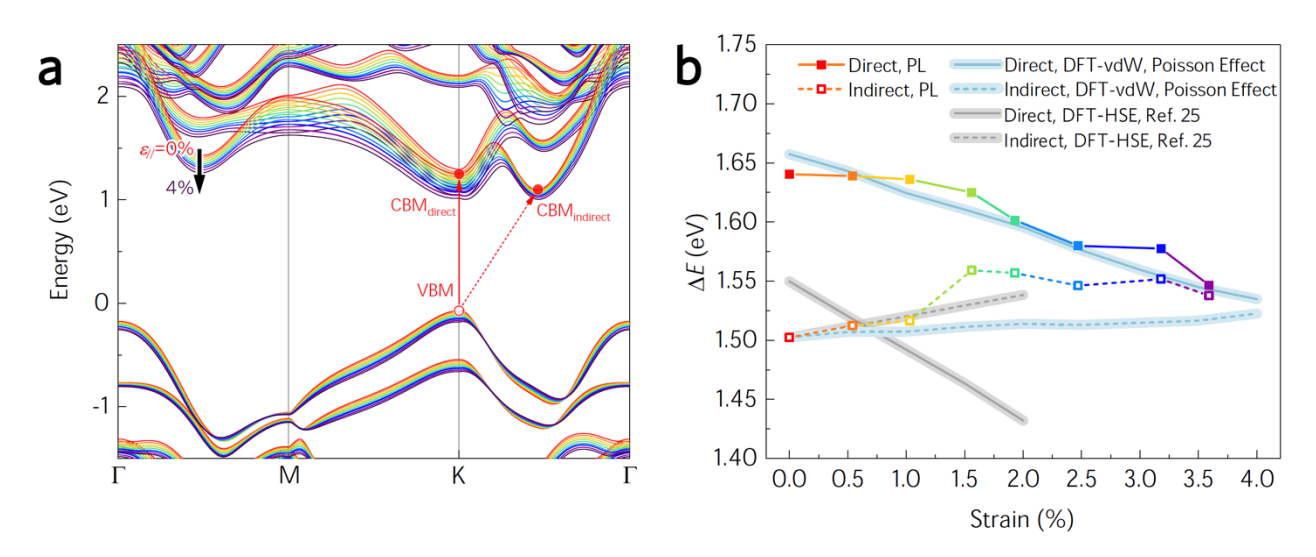


Figure 3. Indirect-to-direct electronic band transition conversion through strain. (a) Evolution of the electronic band structure in response to uniaxial strain calculated using density functional theory including both spin orbit coupling, interlayer van der Waals interactions, and the Poisson effect (DFT-vdW-Poisson) for  $\varepsilon_{\parallel} = 0\%$  (red) to 4% (purple) in increments of 0.5%. Direct and indirect electronic transitions are depicted. (b) Strain-dependence of the interband transition energies normalized to that of the unstrained indirect PL transition. Experimental values have been obtained by deconvolution of the PL emission spectra using Gaussian distributions and are shown in comparison with a DFT-vdW-Poisson model and a calculation neglecting van der Waals interactions (DFT-HSE<sup>25</sup>). The indirect-to-direct conversion occurs at  $\varepsilon_{\parallel} > 3.5\%$  in both the experiment and DFT-vdW-Poisson calculation and at  $\sim$ 0.5% when vdW interactions are neglected (DFT-HSE<sup>25</sup>), indicating that increased interlayer coupling strength may lead to weaker strain-coupled effects in layered materials.

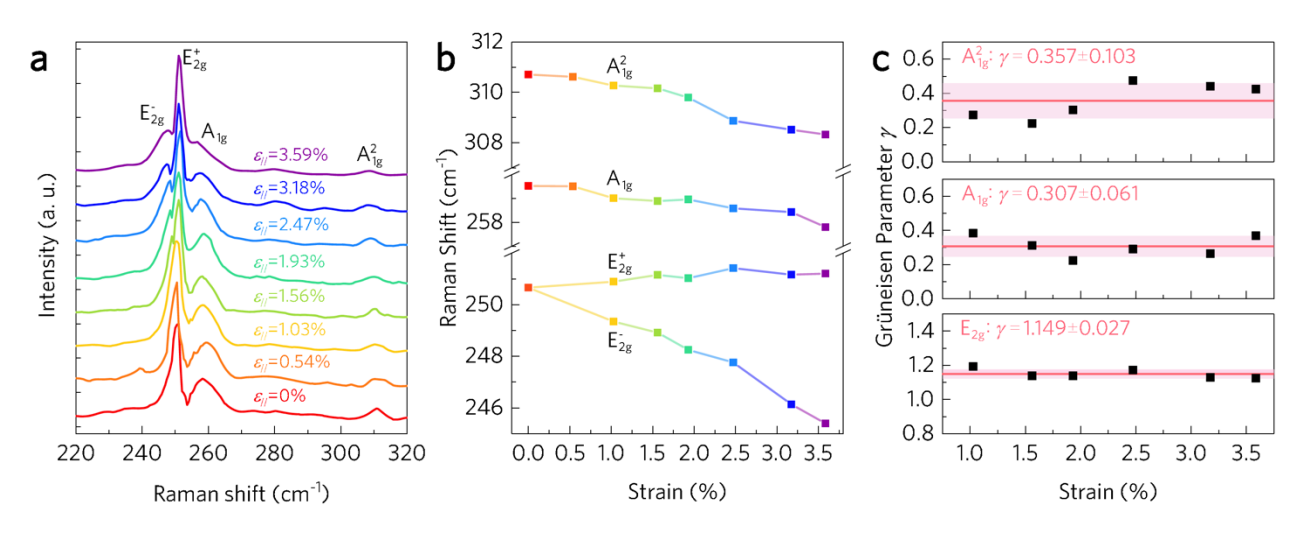
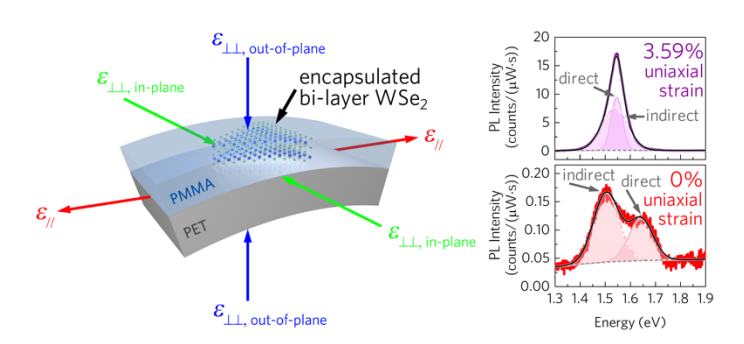


Figure 4. Raman spectra of bilayer WSe<sub>2</sub> as it is strained up to 3.59%. (a) Raman spectra as a function of uniaxial strain ( $\varepsilon_{l/l}$ ). As strain increases, the in-plane  $E_{2g}$  optical phonon mode evolves into separate  $E_{2g}^+$  and  $E_{2g}^-$  modes. (b) Strain dependence of the peak Raman shifts for the  $E_{2g}^+$ ,  $E_{2g}^-$ ,  $A_{1g}^-$ , and  $A_{1g}^2$  modes, obtained by deconvolution of the experimental Raman spectra using Lorentzian distributions. The linear strain dependence of the Raman shift indicates strain relaxation by slippage or plastic deformation is not observed. (c) Mode-specific Grüneisen parameters of bilayer WSe<sub>2</sub> are constant over the range of  $0.01 \le \varepsilon_{l/l} \le 0.036$ .



**Figure for Table of Contents.** 

